Biomedical Optics EXPRESS

Simultaneous FRAP, FLIM and FAIM for measurements of protein mobility and interaction in living cells

James A. Levitt,[1] Penny E. Morton,[2,4] Gilbert O. Fruhwirth,[3] George Santis,[2] Pei-Hua Chung,[1] Maddy Parsons,[4] and Klaus Suhling[1,*]

[1]Department of Physics, King's College London, Strand, London WC2R 2LS, UK
[2]Division of Asthma, Allergy, and Lung Biology, Guys Campus, King's College London, London, UK
[3]Department of Imaging Chemistry and Biology, Division of Imaging Sciences and Biomedical Engineering, St. Thomas Hospital, King's College London, SE1 7EH, UK
[4]Randall Division of Cell and Molecular Biophysics, Guys Campus, King's College London, London, SE1 1UL, UK
[*]klaus.suhling@kcl.ac.uk

Abstract: We present a novel integrated multimodal fluorescence microscopy technique for simultaneous fluorescence recovery after photobleaching (FRAP), fluorescence lifetime imaging (FLIM) and fluorescence anisotropy imaging (FAIM). This approach captures a series of polarization-resolved fluorescence lifetime images during a FRAP recovery, maximizing the information available from a limited photon budget. We have applied this method to analyse the behaviour of GFP-labelled coxsackievirus and adenovirus receptor (CAR) in living human epithelial cells. Our data reveal that CAR exists in oligomeric states throughout the cell, and that these complexes occur in conjunction with high immobile fractions of the receptor at cell-cell junctions. These findings shed light on previously unknown molecular associations between CAR receptors in intact cells and demonstrate the power of combined FRAP, FLIM and FAIM microscopy as a robust method to analyse complex multi-component dynamics in living cells.

©2015 Optical Society of America

OCIS codes: (180.0180) Microscopy; (300.0300) Spectroscopy; (170.2520) Fluorescence microscopy; (170.6920) Time-resolved imaging; (260.2160) Energy transfer; (260.5430) Polarization

References and links

1. J. A. Levitt, D. R. Matthews, S. M. Ameer-Beg, and K. Suhling, "Fluorescence lifetime and polarization-resolved imaging in cell biology," Curr. Opin. Biotechnol. **20**(1), 28–36 (2009).
2. J. W. Borst and A. J. W. G. Visser, "Fluorescence lifetime imaging microscopy in life sciences," Meas. Sci. Technol. **21**(10), 102002 (2010).
3. W. Becker, "Fluorescence lifetime imaging - techniques and applications," J. Microsc. **247**(2), 119–136 (2012).
4. X. Michalet, O. H. W. Siegmund, J. V. Vallerga, P. Jelinsky, J. E. Millaud, and S. Weiss, "Detectors for single-molecule fluorescence imaging and spectroscopy," J. Mod. Opt. **54**(2-3), 239–281 (2007).
5. J. Lippincott-Schwartz, E. Snapp, and A. Kenworthy, "Studying protein dynamics in living cells," Nat. Rev. Mol. Cell Biol. **2**(6), 444–456 (2001).
6. H. Deschout, K. Raemdonck, J. Demeester, S. C. De Smedt, and K. Braeckmans, "FRAP in Pharmaceutical Research: Practical Guidelines and Applications in Drug Delivery," Pharm. Res. **31**(2), 255–270 (2014).
7. N. Smisdom, K. Braeckmans, H. Deschout, M. vandeVen, J. M. Rigo, S. C. De Smedt, and M. Ameloot, "Fluorescence recovery after photobleaching on the confocal laser-scanning microscope: generalized model without restriction on the size of the photobleached disk," J. Biomed. Opt. **16**(4), 046021 (2011).
8. M. Kang, C. A. Day, K. Drake, A. K. Kenworthy, and E. DiBenedetto, "A Generalization of Theory for Two-Dimensional Fluorescence Recovery after Photobleaching Applicable to Confocal Laser Scanning Microscopes," Biophys. J. **97**(5), 1501–1511 (2009).
9. S. Seiffert and W. Oppermann, "Systematic evaluation of FRAP experiments performed in a confocal laser scanning microscope," J. Microsc. **220**(1), 20–30 (2005).
10. M. A. Rizzo and D. W. Piston, "High-contrast imaging of fluorescent protein FRET by fluorescence polarization microscopy," Biophys. J. **88**(2), L14–L16 (2005).
11. J. Hunt, A. H. Keeble, R. E. Dale, M. K. Corbett, R. L. Beavil, J. Levitt, M. J. Swann, K. Suhling, S. Ameer-Beg, B. J. Sutton, and A. J. Beavil, "A fluorescent biosensor reveals conformational changes in human

#243733 Received 29 Jun 2015; revised 16 Aug 2015; accepted 18 Aug 2015; published 8 Sep 2015

immunoglobulin E Fc: implications for mechanisms of receptor binding, inhibition, and allergen recognition," J. Biol. Chem. **287**(21), 17459–17470 (2012).
12. D. R. Matthews, L. M. Carlin, E. Ofo, P. R. Barber, B. Vojnovic, M. Irving, T. Ng, and S. M. Ameer-Beg, "Time-lapse FRET microscopy using fluorescence anisotropy," J. Microsc. **237**(1), 51–62 (2010).
13. A. N. Bader, E. G. Hofman, J. Voortman, P. M. en Henegouwen, and H. C. Gerritsen, "Homo-FRET Imaging Enables Quantification of Protein Cluster Sizes with Subcellular Resolution," Biophys. J. **97**(9), 2613–2622 (2009).
14. C. Thaler, S. V. Koushik, H. L. Puhl 3rd, P. S. Blank, and S. S. Vogel, "Structural rearrangement of CaMKIIalpha catalytic domains encodes activation," Proc. Natl. Acad. Sci. USA **106**(15), 6369–6374 (2009).
15. A. N. Bader, E. G. Hofman, P. M. van Bergen En Henegouwen, and H. C. Gerritsen, "Imaging of protein cluster sizes by means of confocal time-gated fluorescence anisotropy microscopy," Opt. Express **15**(11), 6934–6945 (2007).
16. V. Devauges, C. Marquer, S. Lécart, J.-C. Cossec, M.-C. Potier, E. Fort, K. Suhling, and S. Lévêque-Fort, "Homodimerization of Amyloid Precursor Protein at the Plasma Membrane: A homoFRET Study by Time-Resolved Fluorescence Anisotropy Imaging," PLoS One **7**(9), e44434 (2012).
17. A. H. A. Clayton, Q. S. Hanley, D. J. Arndt-Jovin, V. Subramaniam, and T. M. Jovin, "Dynamic fluorescence anisotropy imaging microscopy in the frequency domain (rFLIM)," Biophys. J. **83**(3), 1631–1649 (2002).
18. I. Gautier, M. Tramier, C. Durieux, J. Coppey, R. B. Pansu, J. C. Nicolas, K. Kemnitz, and M. Coppey-Moisan, "Homo-FRET microscopy in living cells to measure monomer-dimer transition of GFP-tagged proteins," Biophys. J. **80**(6), 3000–3008 (2001).
19. R. Varma and S. Mayor, "GPI-anchored proteins are organized in submicron domains at the cell surface," Nature **394**(6695), 798–801 (1998).
20. P. Sharma, R. Varma, R. C. Sarasij, K. Ira, K. Gousset, G. Krishnamoorthy, M. Rao, and S. Mayor, "Nanoscale organization of multiple GPI-anchored proteins in living cell membranes," Cell **116**(4), 577–589 (2004).
21. A. M. Melo, A. Fedorov, M. Prieto, and A. Coutinho, "Exploring homo-FRET to quantify the oligomer stoichiometry of membrane-bound proteins involved in a cooperative partition equilibrium," Phys. Chem. Chem. Phys. **16**(34), 18105–18117 (2014).
22. Z. Zolmajd-Haghighi and Q. S. Hanley, "When One Plus One Does Not Equal Two: Fluorescence Anisotropy in Aggregates and Multiply Labeled Proteins," Biophys. J. **106**(7), 1457–1466 (2014).
23. L. W. Runnels and S. F. Scarlata, "Theory and application of fluorescence homotransfer to melittin oligomerization," Biophys. J. **69**(4), 1569–1583 (1995).
24. S. V. Koushik and S. S. Vogel, "Energy migration alters the fluorescence lifetime of Cerulean: implications for fluorescence lifetime imaging Forster resonance energy transfer measurements," J. Biomed. Opt. **13**(3), 031204 (2008).
25. K. Suhling, J. Siegel, P. M. P. Lanigan, S. Lévêque-Fort, S. E. D. Webb, D. Phillips, D. M. Davis, and P. M. W. French, "Time-resolved fluorescence anisotropy imaging applied to live cells," Opt. Lett. **29**(6), 584–586 (2004).
26. J. Siegel, K. Suhling, S. Leveque-Fort, S. E. D. Webb, D. M. Davis, D. Phillips, Y. Sabharwal, and P. M. W. French, "Wide-field time-resolved fluorescence anisotropy imaging (TR-FAIM): Imaging the rotational mobility of a fluorophore," Rev. Sci. Instrum. **74**(1), 182–192 (2003).
27. D. S. Lidke, P. Nagy, B. G. Barisas, R. Heintzmann, J. N. Post, K. A. Lidke, A. H. A. Clayton, D. J. Arndt-Jovin, and T. M. Jovin, "Imaging molecular interactions in cells by dynamic and static fluorescence anisotropy (rFLIM and emFRET)," Biochem. Soc. Trans. **31**(5), 1020–1027 (2003).
28. F. Festy, S. M. Ameer-Beg, T. Ng, and K. Suhling, "Imaging proteins in vivo using fluorescence lifetime microscopy," Mol. Biosyst. **3**(6), 381–391 (2007).
29. W. Becker, A. Bergmann, M. A. Hink, K. König, K. Benndorf, and C. Biskup, "Fluorescence lifetime imaging by time-correlated single-photon counting," Microsc. Res. Tech. **63**(1), 58–66 (2004).
30. P. I. H. Bastiaens and A. Squire, "Fluorescence lifetime imaging microscopy: spatial resolution of biochemical processes in the cell," Trends Cell Biol. **9**(2), 48–52 (1999).
31. K. Suhling, P. M. W. French, and D. Phillips, "Time-resolved fluorescence microscopy," Photochem. Photobiol. Sci. **4**(1), 13–22 (2005).
32. K. Suhling, L. M. Hirvonen, J. A. Levitt, P.-H. Chung, C. Tregidgo, A. Le Marois, D. A. Rusakov, K. Zheng, S. Ameer-Beg, S. Poland, S. Coelho, R. Henderson, and N. Krstajic, "Fluorescence lifetime imaging (FLIM): Basic concepts and some recent developments," Medical Photonics **27**, 3–40 (2015).
33. M. Y. Berezin and S. Achilefu, "Fluorescence Lifetime Measurements and Biological Imaging," Chem. Rev. **110**(5), 2641–2684 (2010).
34. R. Sanders, A. Draaijer, H. C. Gerritsen, P. M. Houpt, and Y. K. Levine, "Quantitative pH imaging in cells using confocal fluorescence lifetime imaging microscopy," Anal. Biochem. **227**(2), 302–308 (1995).
35. K. Suhling, J. Siegel, D. Phillips, P. M. W. French, S. Lévêque-Fort, S. E. D. Webb, and D. M. Davis, "Imaging the environment of green fluorescent protein," Biophys. J. **83**(6), 3589–3595 (2002).
36. C. Tregidgo, J. A. Levitt, and K. Suhling, "Effect of refractive index on the fluorescence lifetime of green fluorescent protein," J. Biomed. Opt. **13**(3), 031218 (2008).
37. H. J. van Manen, P. Verkuijlen, P. Wittendorp, V. Subramaniam, T. K. van den Berg, D. Roos, and C. Otto, "Refractive index sensing of green fluorescent proteins in living cells using fluorescence lifetime imaging microscopy," Biophys. J. **94**(8), L67–L69 (2008).
38. A. Pliss, L. Zhao, T. Y. Ohulchanskyy, J. Qu, and P. N. Prasad, "Fluorescence lifetime of fluorescent proteins as an intracellular environment probe sensing the cell cycle progression," ACS Chem. Biol. **7**(8), 1385–1392 (2012).

#243733 Received 29 Jun 2015; revised 16 Aug 2015; accepted 18 Aug 2015; published 8 Sep 2015

39. M. K. Kuimova, G. Yahioglu, and P. R. Ogilby, "Singlet Oxygen in a Cell: Spatially Dependent Lifetimes and Quenching Rate Constants," J. Am. Chem. Soc. **131**(1), 332–340 (2009).
40. M. K. Kuimova, G. Yahioglu, J. A. Levitt, and K. Suhling, "Molecular rotor measures viscosity of live cells via fluorescence lifetime imaging," J. Am. Chem. Soc. **130**(21), 6672–6673 (2008).
41. J. A. Levitt, M. K. Kuimova, G. Yahioglu, P. H. Chung, K. Suhling, and D. Phillips, "Membrane-Bound Molecular Rotors Measure Viscosity in Live Cells via Fluorescence Lifetime Imaging," J. Phys. Chem. C **113**(27), 11634–11642 (2009).
42. X. Peng, Z. Yang, J. Wang, J. Fan, Y. He, F. Song, B. Wang, S. Sun, J. Qu, J. Qi, and M. Yan, "Fluorescence Ratiometry and Fluorescence Lifetime Imaging: Using a Single Molecular Sensor for Dual Mode Imaging of Cellular Viscosity," J. Am. Chem. Soc. **133**(17), 6626–6635 (2011).
43. M. J. Roberti, T. M. Jovin, and E. Jares-Erijman, "Confocal Fluorescence Anisotropy and FRAP Imaging of α-Synuclein Amyloid Aggregates in Living Cells," PLoS One **6**(8), e23338 (2011).
44. B. W. M. Kuipers, M. C. A. van de Ven, R. J. Baars, and A. P. Philipse, "Simultaneous measurement of rotational and translational diffusion of anisotropic colloids with a new integrated setup for fluorescence recovery after photobleaching," J. Phys. Condens. Matter **24**(24), 245101 (2012).
45. A. S. Klein, M. Schaefer, T. Korte, A. Herrmann, and A. Tannert, "HaCaT keratinocytes exhibit a cholesterol and plasma membrane viscosity gradient during directed migration," Exp. Cell Res. **318**(7), 809–818 (2012).
46. S. Engel, S. Scolari, B. Thaa, N. Krebs, T. Korte, A. Herrmann, and M. Veit, "FLIM-FRET and FRAP reveal association of influenza virus haemagglutinin with membrane rafts," Biochem. J. **425**(3), 567–573 (2010).
47. M. Vitali, M. Reis, T. Friedrich, and H.-J. Eckert, "A wide-field multi-parameter FLIM and FRAP setup to investigate the fluorescence emission of individual living cyanobacteria," Proc. SPIE **7376**, 737610 (2010).
48. D. R. Matthews, G. O. Fruhwirth, G. Weitsman, L. M. Carlin, E. Ofo, M. Keppler, P. R. Barber, I. D. C. Tullis, B. Vojnovic, T. Ng, and S. M. Ameer-Beg, "A Multi-Functional Imaging Approach to High-Content Protein Interaction Screening," PLoS One **7**(4), e33231 (2012).
49. Y. Zhou, J. M. Dickenson, and Q. S. Hanley, "Imaging lifetime and anisotropy spectra in the frequency domain," J. Microsc. **234**(1), 80–88 (2009).
50. J. A. Levitt, P.-H. Chung, D. R. Alibhai, and K. Suhling, "Simultaneous measurements of fluorescence lifetimes, anisotropy and FRAP recovery curves," Proc. SPIE **7902**, 79020Y (2011).
51. J. M. Bergelson, J. A. Cunningham, G. Droguett, E. A. Kurt-Jones, A. Krithivas, J. S. Hong, M. S. Horwitz, R. L. Crowell, and R. W. Finberg, "Isolation of a common receptor for Coxsackie B viruses and adenoviruses 2 and 5," Science **275**(5304), 1320–1323 (1997).
52. C. J. Cohen, J. T. C. Shieh, R. J. Pickles, T. Okegawa, J. T. Hsieh, and J. M. Bergelson, "The coxsackievirus and adenovirus receptor is a transmembrane component of the tight junction," Proc. Natl. Acad. Sci. U.S.A. **98**(26), 15191–15196 (2001).
53. K. J. Excoffon, A. Hruska-Hageman, M. Klotz, G. L. Traver, and J. Zabner, "A role for the PDZ-binding domain of the coxsackie B virus and adenovirus receptor (CAR) in cell adhesion and growth," J. Cell Sci. **117**(19), 4401–4409 (2004).
54. C. Patzke, K. E. A. Max, J. Behlke, J. Schreiber, H. Schmidt, A. A. Dorner, S. Kröger, M. Henning, A. Otto, U. Heinemann, and F. G. Rathjen, "The Coxsackievirus-Adenovirus Receptor Reveals Complex Homophilic and Heterophilic Interactions on Neural Cells," J. Neurosci. **30**(8), 2897–2910 (2010).
55. M. J. van Raaij, E. Chouin, H. van der Zandt, J. M. Bergelson, and S. Cusack, "Dimeric structure of the coxsackievirus and adenovirus receptor D1 domain at 1.7 A resolution," Structure **8**(11), 1147–1155 (2000).
56. R. D. Ramirez, S. Sheridan, L. Girard, M. Sato, Y. Kim, J. Pollack, M. Peyton, Y. Zou, J. M. Kurie, J. M. Dimaio, S. Milchgrub, A. L. Smith, R. F. Souza, L. Gilbey, X. Zhang, K. Gandia, M. B. Vaughan, W. E. Wright, A. F. Gazdar, J. W. Shay, and J. D. Minna, "Immortalization of human bronchial epithelial cells in the absence of viral oncoproteins," Cancer Res. **64**(24), 9027–9034 (2004).
57. C. Farmer, P. E. Morton, M. Snippe, G. Santis, and M. Parsons, "Coxsackie adenovirus receptor (CAR) regulates integrin function through activation of p44/42 MAPK," Exp. Cell Res. **315**(15), 2637–2647 (2009).
58. C. Demaison, K. Parsley, G. Brouns, M. Scherr, K. Battmer, C. Kinnon, M. Grez, and A. J. Thrasher, "High-level transduction and gene expression in hematopoietic repopulating cells using a human immunodeficiency virus type 1-based lentiviral vector containing an internal spleen focus forming virus promoter," Hum. Gene Ther. **13**(7), 803–813 (2002).
59. P. R. Barber, S. M. Ameer-Beg, J. Gilbey, L. M. Carlin, M. Keppler, T. C. Ng, and B. Vojnovic, "Multiphoton time-domain fluorescence lifetime imaging microscopy: practical application to protein-protein interactions using global analysis," J. R. Soc. Interface **6**(Suppl_1), S93–S105 (2009).
60. A. C. Ribou, J. Vigo, and J. M. Salmon, "Synthesis and characterization of (1 "-pyrene butyl)-2-rhodamine ester: a new probe for oxygen measurement in the mitochondria of living cells," J. Photochem. Photobiol. Chem. **151**(1-3), 49–55 (2002).
61. A. J. Cross and G. R. Fleming, "Analysis of time-resolved fluorescence anisotropy decays," Biophys. J. **46**(1), 45–56 (1984).
62. D. Axelrod, "Carbocyanine dye orientation in red cell membrane studied by microscopic fluorescence polarization," Biophys. J. **26**(3), 557–573 (1979).
63. A. Squire, P. J. Verveer, O. Rocks, and P. I. H. Bastiaens, "Red-edge anisotropy microscopy enables dynamic imaging of homo-FRET between green fluorescent proteins in cells," J. Struct. Biol. **147**(1), 62–69 (2004).
64. E. Sherman, A. Itkin, Y. Y. Kuttner, E. Rhoades, D. Amir, E. Haas, and G. Haran, "Using fluorescence correlation spectroscopy to study conformational changes in denatured proteins," Biophys. J. **94**(12), 4819–4827 (2008).

#243733 Received 29 Jun 2015; revised 16 Aug 2015; accepted 18 Aug 2015; published 8 Sep 2015
(C) 2015 OSA

65. P. O. Gendron, F. Avaltroni, and K. J. Wilkinson, "Diffusion Coefficients of Several Rhodamine Derivatives as Determined by Pulsed Field Gradient-Nuclear Magnetic Resonance and Fluorescence Correlation Spectroscopy," J. Fluoresc. **18**(6), 1093–1101 (2008).
66. F. Hussain, P. E. Morton, M. Snippe, J. Sullivan, C. Farmer, M. L. Martin-Fernandez, M. Parsons, and G. Santis, "CAR Modulates E-Cadherin Dynamics in the Presence of Adenovirus Type 5," PLoS One **6**(8), e23056 (2011).
67. M. Peter, S. M. Ameer-Beg, M. K. Y. Hughes, M. D. Keppler, S. Prag, M. Marsh, B. Vojnovic, and T. Ng, "Multiphoton-FLIM quantification of the EGFP-mRFP1 FRET pair for localization of membrane receptor-kinase interactions," Biophys. J. **88**(2), 1224–1237 (2005).
68. B. Treanor, P. M. P. Lanigan, S. Kumar, C. Dunsby, I. Munro, E. Auksorius, F. J. Culley, M. A. Purbhoo, D. Phillips, M. A. A. Neil, D. N. Burshtyn, P. M. W. French, and D. M. Davis, "Microclusters of inhibitory killer immunoglobulin-like receptor signaling at natural killer cell immunological synapses," J. Cell Biol. **174**(1), 153–161 (2006).
69. E. K. L. Yeow and A. H. A. Clayton, "Enumeration of oligomerization states of membrane proteins in living cells by homo-FRET spectroscopy and microscopy: Theory and application," Biophys. J. **92**(9), 3098–3104 (2007).
70. M. Canel, A. Serrels, D. Miller, P. Timpson, B. Serrels, M. C. Frame, and V. G. Brunton, "Quantitative In vivo imaging of the effects of inhibiting integrin signaling via SRC and FAK on cancer cell movement: effects on E-cadherin dynamics," Cancer Res. **70**(22), 9413–9422 (2010).
71. K. A. Lidke, B. Rieger, D. S. Lidke, and T. M. Jovin, "The role of photon statistics in fluorescence anisotropy imaging," IEEE Trans. Image Process. **14**(9), 1237–1245 (2005).
72. J. M. Carvajal-Gonzalez, D. Gravotta, R. Mattera, F. Diaz, A. Perez Bay, A. C. Roman, R. P. Schreiner, R. Thuenauer, J. S. Bonifacino, and E. Rodriguez-Boulan, "Basolateral sorting of the coxsackie and adenovirus receptor through interaction of a canonical YXXPhi motif with the clathrin adaptors AP-1A and AP-1B," Proc. Natl. Acad. Sci. U.S.A. **109**(10), 3820–3825 (2012).
73. S. Terrillon and M. Bouvier, "Roles of G-protein-coupled receptor dimerization - From ontogeny to signalling regulation," EMBO Rep. **5**(1), 30–34 (2004).

1. Introduction

Fluorescence microscopy is an essential tool for live cell imaging yielding information on macromolecular structure, location, interactions and dynamics. The fluorescence spectrum, intensity, lifetime, polarization and their evolution in time can provide a wealth of information about intracellular environments and their dynamics [1–3]. Capturing as many of these features as possible in a single measurement maximises the information extracted from the sample and ensures that the limited photon budget available from each fluorophore is used effectively. Living cells show dynamic behaviour over a wide range of timescales – from sub-nanosecond conformational fluctuations to chemical reactions and interactions over several hours [4]. Protein mobility can be measured using a variety of fluorescence microscopy techniques. For example, fluorescence recovery after photobleaching (FRAP), in which the fluorescence intensity in a region of interest is measured as a function of time following rapid, irreversible photobleaching, can report on translational intracellular protein mobility [5, 6]. Such experiments are relatively straightforward to perform and methods for analysis are becoming increasingly more sophisticated, with general models for calculations of diffusion coefficients from confocal FRAP experiments [7–9]. The rotational mobility of fluorophores can be probed by measuring the emission polarized parallel and perpendicular to the excitation light and calculating the fluorescence anisotropy. This approach can also be used to identify Förster resonance energy transfer (FRET) between both different fluorophore types [10–12] and between the same type of fluorophores (i.e. homo-FRET or emFRET) [13–23]. In fact, with rare exceptions, e.g. [24], fluorescence anisotropy can be the only method to identify homo-FRET if the two fluorophores are in the same environment and their lifetimes are identical. Time-resolved fluorescence anisotropy imaging (tr-FAIM) [17, 25–27] is currently rarely used in biology but has potential to be a powerful indicator of rotational diffusion of fluorophores, protein structure or function [1]. Underpinning tr-FAIM, fluorescence lifetime imaging microscopy (FLIM) [2, 3, 28–33] maps the fluorescence lifetime in every pixel of an image and is a powerful technique for probing the local environment of a fluorophore as the measured lifetime is largely independent of fluorophore concentration, but can be sensitive to pH [34], refractive index [35–38], reactive quenching species [39] and viscosity [30, 31, 40–42]. Both fluorescence anisotropy and FRAP have previously been used independently for a study of aggregation states of alpha-synuclein, a protein which plays a role in Parkinson's disease [43], and an arrangement for dynamic FRAP

#243733 Received 29 Jun 2015; revised 16 Aug 2015; accepted 18 Aug 2015; published 8 Sep 2015
(C) 2015 OSA

and rotational diffusion measurements for colloids has been presented [44]. FRAP and FLIM have also recently been used independently in a study of keratinocyte migration [45], influenza virus association with lipid rafts [46], and cyanobacteria [47]. FLIM and anisotropy have recently been used for high content screening [48], and a system for widefield spectrally-resolved fluorescence lifetime and anisotropy imaging has been presented [49]. However, to our knowledge there has not yet been an example of FLIM, FRAP and FAIM used simultaneously in combination for studies of protein dynamics.

In living samples undergoing continuous change it is desirable to extract the maximum amount of information available whilst minimising exposure to intense light and reducing the effects of photobleaching, phototoxicity and varying sample morphology due to motion on the measurements by keeping acquisition times short. As such, it is beneficial to combine measurements rather than perform many consecutive measurements on a sample. To address this issue and in an effort to maximise the amount of information obtained from a single experiment we have combined three fluorescence microscopy techniques [50], as schematically illustrated in Fig. 1. Our experimental set-up is based on an inverted laser scanning confocal microscope with time-correlated single photon counting (TCSPC) detection using hybrid GaAsP photomultiplier detectors. This allows for FLIM, FRAP and tr-FAIM experiments to be performed simultaneously, rather than sequentially, for the same photon budget, and with the same acquisition times and spatial resolution as a typical FLIM experiment, whilst retaining all of the benefits of each individual fluorescence technique. The time-resolution for the FRAP recovery curves is on the timescale of seconds which is well suited to monitoring protein dynamics in membranes. The anisotropy measurements allow for identification of species undergoing FRET and the fluorescence lifetime measurements have the potential to allow identification of local variations in the fluorophore environment. This approach is useful, for example, for distinguishing between high local fluorophore concentrations and oligomeric structures.

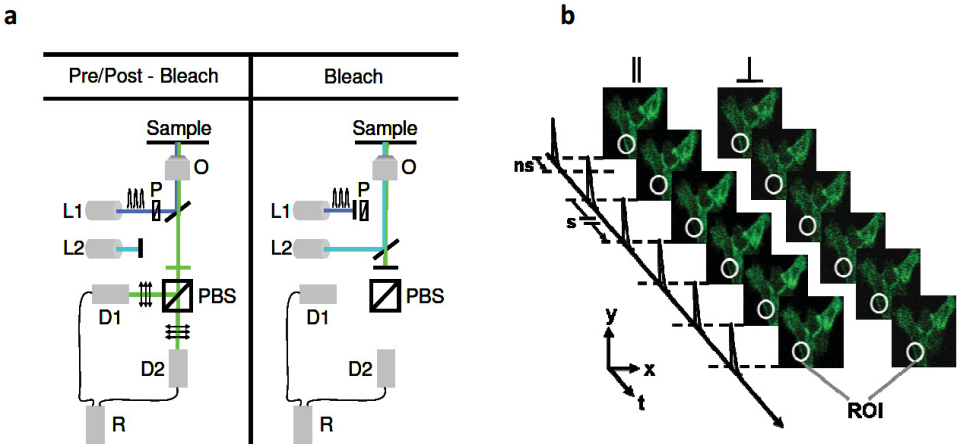

Fig. 1. (a) Experimental arrangement for combined FRAP, FLIM, tr-FAIM. The FRAP experiment is performed in three stages – pre-bleach, bleach and post-bleach. L1: pulsed diode laser; L2: continuous wave laser; P: polarizer; O: 63 × NA1.2 objective lens; PBS: polarizing beamsplitter cube; D1 and D2: GaAsP hybrid detectors; R: signal router. (b) The resulting data set is comprised of a series of pairs of time and polarization-resolved (|| and ⊥) fluorescence images with nanosecond time resolution, with a photobleached ROI in each image, which are then processed and analysed to extract FRAP recovery curves, FLIM and FAIM maps. Pairs of images are recorded at intervals of ~3.5 s.

We have measured fluorescence lifetimes, depolarization, and translational mobility of coxsackievirus and adenovirus receptor (CAR) [51] labelled with GFP in living human bronchial epithelial cells (HBEC) simultaneously in the same experiment. CAR is a

#243733 Received 29 Jun 2015; revised 16 Aug 2015; accepted 18 Aug 2015; published 8 Sep 2015
(C) 2015 OSA

transmembrane protein that localises to cell-cell junctions and is proposed to play a role in mediating cell-cell adhesion [52, 53]. The extracellular N-terminal domain of CAR is known to exist as a homo-dimer in solution and various biochemical evidence suggest this may contribute to *cis* and *trans* interactions between receptors, i.e. within the same cell and across cell-cell junctions [51–54]. However, the receptor state in intact cells and the potential role of self-association in controlling cell-cell adhesion and adenovirus docking is currently unknown [54, 55]. We have therefore applied combined FRAP, FLIM, tr-FAIM microscopy to investigate the dynamics and dimerisation of CAR in living cells.

2. Experimental

2.1 Preparation of rhodamine 123 samples

All materials were used as received and solvents were spectrophotometric grade. A stock solution of 1.3 mM rhodamine 123 (rh123, M_w = 380.82, Sigma, UK) in methanol (Sigma Aldrich, UK) was made and 40 µl of the stock solution was added to a 10 ml mixture of glycerol (Sigma Aldrich, UK) and methanol with volume fraction 90:10 to give a final concentration of the dye 5.2 µM. For imaging, 200 µl of the solution was imaged in one well of a 96-well plate with a coverglass underside (Whatman) at room temperature.

2.2 Cell culture and preparation

Cells were cultured on a 6-well plate as part of a resistively-heated micro-incubation system (SmartSlide50, Wafergen, UK). For imaging the cells were heated to 37 °C and 5% CO_2 / 95% air was flowed through the well. Immortalised human bronchial epithelial cells (HBEC) were a gift from Dr Jerry Shay (UT Southwestern [56]) and were grown in keratinocyte serum-free media (KSFM; Invitrogen). CAR-GFP expressing stable cell lines were produced using lentiviral expression. CAR-GFP lentivirus particles were generated in 293T packaging cells (as in ref [53].) and these cells were maintained in DMEM containing 10% FCS, supplemented with glutamine. Plasmids encoding full-length CAR have been described previously [57]. Full length CAR-GFP was cloned in frame into pHR9SIN-SEW lentiviral expression vector, which was a gift from Dr Adrian Thrasher (Institute of Child Health, UCL, London [58]), and into pGEX-2T. Cells were plated at high density onto custom designed 6-well plates (SmartSlide50, Wafergen, UK) 36 hours prior to analysis. For control experiments HBEC were transiently transfected with eGFP-N1 (Clontech) using Fugene 6 (Roche) according to the manufacturer's instructions and imaged 36 hours post-transfection.

2.3 Combined FRAP, FLIM, tr-FAIM microscopy

The microscopy experiments were performed using an inverted confocal laser scanning microscope (Leica TCS SP2). Samples were imaged using a 63 × water immersion objective (NA 1.2, heated to 37 °C) with a line scan speed of 400 Hz (1.64 s per frame) Two lasers were used for the FRAP experiment – a pulsed diode laser at 467 nm (Hamamatsu PLP 10) with pulse duration of 90 ps, repetition rate of 20 MHz and average power ~1µW for the pre- and post-bleach imaging, and a continuous wave Ar^+ laser at 488 nm with an average power of ~1 mW for the bleach frame. A time-lapse acquisition series was set up with three pre-bleach frames, followed by one bleach frame of duration 1.64 s, and then post-bleach frames which were looped until the FRAP recovery was complete and the image acquisition was terminated. The repetition rate of the diode laser gave a 50 ns window for acquisition of fluorescence decays and thus the advantage of being able to record complete decays from rh123 and GFP. The fluorescence was passed through a polarizing beamsplitter cube and the orthogonally polarized components were detected using two GaAsP hybrid detectors (Becker & Hickl HPM-100-40). The signal from the detectors was fed via a router into a time-correlated single photon counting board (SPC-830 Becker & Hickl) and time and polarization-resolved images (256 x 128 pixels) were recorded with 256 time channels. Typically, 100 - 150 pairs of images recorded per experiment which resulted in a total acquisition time of ~300 – 450 s per experiment. Additional fluorescence anisotropy

#243733 Received 29 Jun 2015; revised 16 Aug 2015; accepted 18 Aug 2015; published 8 Sep 2015
(C) 2015 OSA

measurements of HBEC expressing CAR-GFP and control measurements of HBEC expressing empty vector GFP constructs were performed with an upgraded system using two SPC-150 photon counting boards (Becker & Hickl).

2.4 Data analysis

Analysis of the data was performed using TRI2 time-resolved image analysis software [59]. For the FRAP recovery curve each pair of images recorded in each frame was summed to give an image of the total measured intensity per frame. The bleached ROI was masked and the intensity was obtained by adding the photon counts. The intensity was corrected for bleaching and fluctuations by measuring the intensity in another region of the image where the cells were immobile on the time scale of the experiment. The recovery curves were fitted to a monoexponential recovery curve. The FLIM images were created by summing all of the measured parallel and perpendicular frames, respectively, and combining them according to the denominator of Eq. (1). We have verified that even for a high NA microscope objective this is valid for fluorescence lifetime measurements. A 50 ns window for fluorescence decays ensures that we measure complete fluorescence decays from GFP. Steady-state anisotropy images were created using the summed parallel and summed perpendicular images an anisotropy macro in TRI2 which processed the images according to Eq. (1). Time-resolved anisotropy decays were measured by integrating the fluorescence over all pixels in the time and polarization images. For FLIM binning of 7x7 pixels was used.

A FRAP recovery curve is measured from a region of interest (ROI) using intensity values from pairs of time and polarization-resolved fluorescence images recorded at regular intervals following photobleaching. Fluorescence anisotropy maps are produced by processing the summed images for each measured polarization component according to Eq. (1), where I_{para} and I_{perp} are the intensity values for fluorescence polarized parallel and perpendicular to the incident radiation, respectively, and G accounts for the difference in detection efficiency for the two measured polarization states.

$$r(t) = \frac{I_{para}(t) - GI_{perp}(t)}{I_{para}(t) + 2GI_{perp}(t)} \tag{1}$$

Combining the time and polarization-resolved images according to the denominator of Eq. (1) and fitting the fluorescence decays in each pixel using an exponential decay model yields a FLIM image. Therefore, during the course of the polarization-resolved FLIM measurements it is possible to extract quantitative translational and homo-FRET oligomerization data and measure fluorescence lifetimes and homo-FRET without extending the acquisition or exposure times used for a typical confocal FLIM experiment.

2.5 Generation of rotational correlation time image and histogram

The rotational correlation time image and histogram for the homogeneous solution sample of rh123 were generated using OptiSP$_e$C software from Becker & Hickl. Briefly, the software is capable of summing multiple time-resolved image files, and we used this function to import and sum 150 images from each of the parallel and perpendicular polarization detection channels. Using spatial binning of 15x15 pixels and a G-factor of 1.35 the fluorescence decays recorded for each polarization in each pixel were fitted simultaneously according using Eq. (2) and Eq. (3) [61].

$$F_{\parallel}(t) = \frac{1}{3}\left[1 + 2r(t)\right] I(t) \otimes R(t + t_s) \tag{2}$$

$$F_{\perp}(t) = \frac{1}{3}\left[1 - r(t)\right] I(t) \otimes R(t + t_s) \tag{3}$$

#243733 Received 29 Jun 2015; revised 16 Aug 2015; accepted 18 Aug 2015; published 8 Sep 2015
(C) 2015 OSA

where $F_{\parallel}$ and $F_{\perp}$ are the fluorescence decays for polarizations parallel and perpendicular to the incident radiation, respectively. *I(t)* and *r(t)* are the time-dependent fluorescence intensity and anisotropy, respectively, *G* accounts for the difference in detection efficiencies of each polarization component, and *R* is the instrument response function (IRF) with t_s the time shift between the IRF and the fluorescence data.

3. Results

3.1 Combined FRAP, FLIM, tr-FAIM microscopy of rhodamine 123 in solution

We first used the combined microscopy set-up to measure fluorescence lifetime, τ_f, and diffusion properties of the well-characterised dye rh123 in a 90:10 (v/v) mixture of glycerol and methanol (viscosity, η = 400 ± 30 cP, refractive index, n = 1.46). The FLIM image (Fig. 2(a)) shows a uniform distribution of fluorescence lifetimes as expected from a dye in homogeneous solution. A typical rh123 fluorescence decay, with τ_f = 3.19 ± 0.07 ns (χ^2 = 1.15), is shown in Fig. 2(a) (inset). The fluorescence lifetime histogram is symmetric and well fitted by a Gaussian distribution centred around 3.25 ns with a full width at half maximum (FWHM) of 0.4 ns. This is in good agreement with the expected value in a high refractive index methanol/glycerol medium (n = 1.46) based on the Strickler-Berg relationship between lifetime and refractive index and the reported lifetime in ref [60]. The steady-state fluorescence anisotropy, *r*, image is shown in Fig. 2(b). This was created by summing the series of images recorded for each polarization state (parallel and perpendicular) and calculating the anisotropy from the intensity values, $I_{\parallel}$ and $I_{\perp}$, in each pixel using Eq. (1). The image is similarly uniform and the fluorescence anisotropy histogram (Fig. 2(b)) is also symmetric and can be fitted to a Gaussian function centred around 0.236 with a FWHM of 0.07.

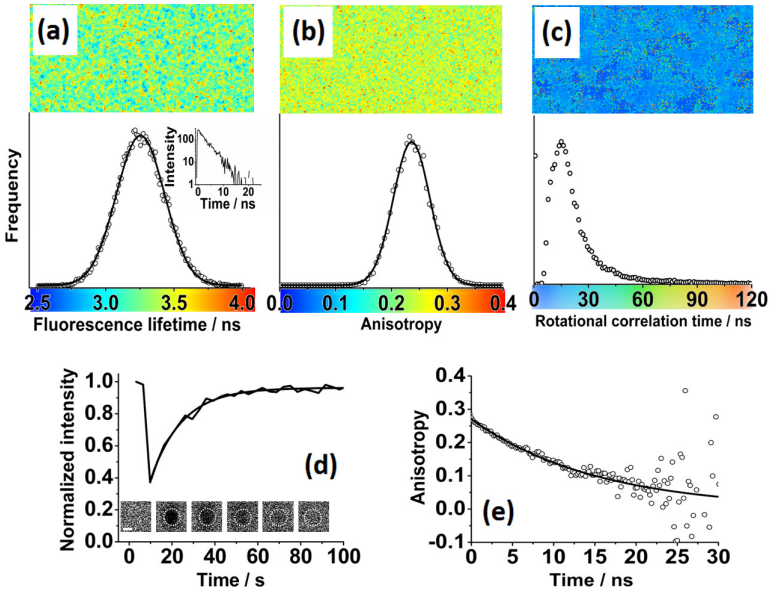

Fig. 2. Representative data set from a single combined FRAP, FLIM, tr-FAIM microscopy experiment measuring rh123 in a 90% V/V glycerol-methanol mixture. (a) FLIM image and fluorescence lifetime histogram (with representative fluorescence decay from a 7x7 pixel region, inset) showing a symmetric distribution (Gaussian fit, black line) of fluorescence lifetimes centred around 3.25 ns. (b) Steady-state fluorescence anisotropy image and histogram with a symmetric distribution (Gaussian fit, black line) centred around 0.24. (c) Rotational correlation time map and histogram with a peak at ~15 ns, (d) FRAP recovery curve with selected fluorescence images (inset) recorded during the experiment. (e) Time-resolved fluorescence anisotropy decay created from the integrated intensity over the entire image. Scale bar 10 μm.

#243733 Received 29 Jun 2015; revised 16 Aug 2015; accepted 18 Aug 2015; published 8 Sep 2015
(C) 2015 OSA

A map of the rotational correlation time (average tumbling time), τ_c, is created for the solution sample (Fig. 2c) by fitting of the polarization-resolved fluorescence decays using OptiSP$_e$C software (Becker & Hickl,) with pixel binning of 15 x 15 pixels. This software allows the determination of rotational correlation times for freely rotating fluorophores by simultaneously fitting both of the polarization-resolved fluorescence decays (Eq. (2) and Eq. (3)) in each pixel [61]. The image shows a homogeneous distribution of rotational correlation times, τ_c, with a peak in the histogram at ~15 ns. The value of τ_c for the dye in the solution, obtained from a monoexponential fit to the fluorescence anisotropy decay curve (Fig. 2(e)) with integrated pixel intensities over the whole image is $\tau_c = 15.2 \pm 2.8$ ns. Using Eq. (4)

$$D_{rot} = \frac{1}{6\tau_c} = \frac{k_b T}{8\eta\pi r^3} \tag{4}$$

where k_b is the Boltzmann constant, T is absolute temperature, η is viscosity, and r is the hydrodynamic radius of the dye, the calculated rotational diffusion coefficient, $D_{rot} = 0.011 \pm 0.002$ ns^{-1}. The initial anisotropy, $r_0 = 0.28 \pm 0.01$ is lower than the theoretical maximum of 0.4 for single photon excitation due to depolarization by the high numerical aperture objective, an effect that has been observed previously [17, 62, 63].

The FRAP recovery curve (Fig. 2(d) with selected images from the recovery image series, inset) can be adequately fitted by a single exponential function with a half time for the fluorescence recovery, $t_{1/2} = 11.5 \pm 0.5$ s and no immobile fraction, as expected for a dye in solution. This is indicative of free diffusion. Assuming Stokes-Einstein-Debye behaviour and using Eq. (5),

$$D_{trans} = \frac{\gamma w^2}{4t_{1/2}} = \frac{k_b T}{6\pi\eta r} \tag{5}$$

where γ is a beam geometry parameter ($\gamma = 0.88$ for a circular beam bleach), w is the radius of the bleach area and $t_{1/2}$ is the half time of the fluorescence recovery, the calculated translational diffusion coefficient is $D_{trans} = 1.8 \pm 0.2$ μm^{2}s^{-1}.

The radius, r, of the rh123 molecule was calculated from the rearranged Stokes-Einstein-Debye equations for translational and rotational diffusion (Eq. (6) and Eq. (7)),

$$r = \frac{k_b T}{6\pi\eta D_{trans}} \tag{6}$$

$$r = \left(\frac{k_b T}{8\eta\pi D_{rot}} \right)^{1/3} \tag{7}$$

yielding values of ~3.1 ± 0.4 Å and ~3.4 ± 0.2 Å for the radius of rh123, respectively, which are in good agreement with values calculated from literature values of the diffusion coefficient of rhodamine dyes [64, 65].

3.2 Combined FRAP, FLIM, tr-FAIM microscopy of CAR-GFP in living human epithelial cells

Having validated our set-up on rh123 in solution, we used it to measure the fluorescence lifetimes, FRAP recovery curves and time-resolved fluorescence anisotropy of CAR-GFP stably expressed in living human bronchial epithelial cells (HBEC). For an acquisition time of ~450 s we recorded a series of 150 pairs of time- and polarization-resolved confocal fluorescence images simultaneously during a single FRAP experiment. The CAR-GFP signal was localised to both cell-cell junctions and within perinuclear compartments in line with previous studies [53, 57]. The tagged receptor has also previously been shown to function in an identical fashion to untagged CAR and fully supports adenovirus type5 infection, binding

#243733 Received 29 Jun 2015; revised 16 Aug 2015; accepted 18 Aug 2015; published 8 Sep 2015
(C) 2015 OSA

to known interaction partners like multi PDZ domain protein 1 (MUPP-1), and cell-cell junction formation [57, 66]. The confocal fluorescence and transmitted light images (Figs. 3(a) and 3(b), respectively) show several cells in the field of view with striated cell-cell junctions (examples shown with white arrows). The FLIM image, and accompanying lifetime

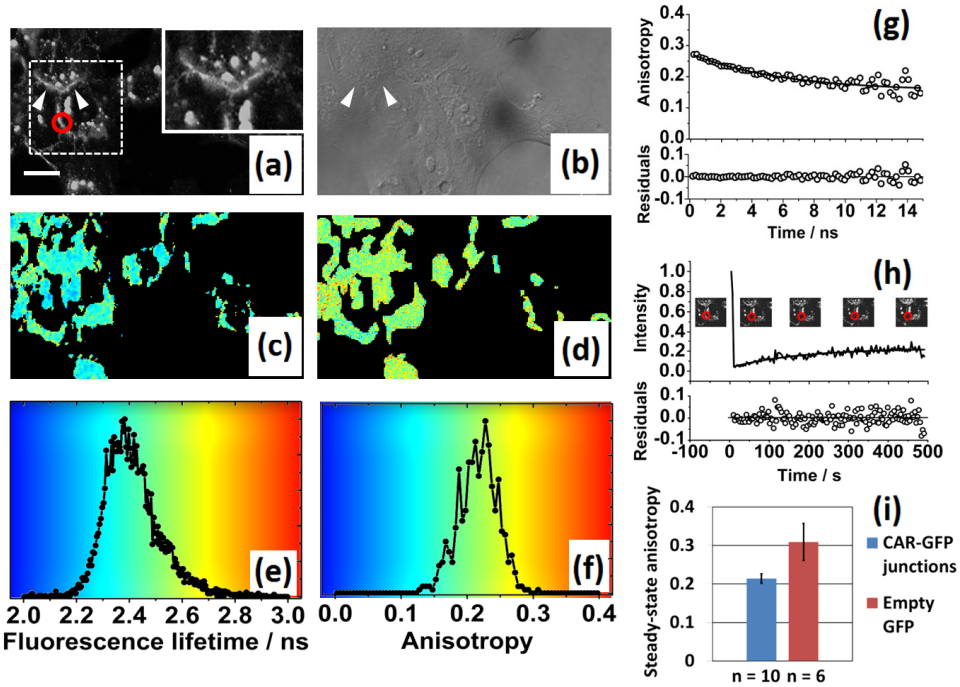

Fig. 3. Representative data set from a single combined FRAP, FLIM, tr-FAIM microscopy experiment measuring CAR-GFP in living HBEC cells. (a) Confocal fluorescence with red circle indicating the bleached region for the FRAP experiments (inset in top right corner shows zoom image of the cell-cell junctions indicated by white arrows). (b) transmitted light images (white arrows indicate cell junctions). (c) FLIM and (d) steady-state anisotropy images with corresponding histograms (e) and (f), respectively. (g) The time-resolved anisotropy decay and (h) FRAP recovery curve (h) shows an appreciable immobile fraction of ~85% and $t_{1/2}$ = 145 ± 25 s. The FRAP recovery images displayed are from the area outlined by the white dashed line in (a).(i) Steady-state anisotropy values in HBEC cells expressing monomeric empty vector GFP and junctions in HBEC cells expressing CAR-GFP. All data in this figure were acquired in 500 s. Scale bar 10 μm.

histogram (Figs. 3(c) and 3(e), respectively) show that the fluorescence lifetimes are fairly uniform across the cells with a peak in the histogram of the GFP lifetimes at τ_f = 2.38 ns, consistent with previous measurements of intracellular GFP [35, 36, 67, 68] and our previous FLIM measurements of CAR-GFP alone [57]. The steady-state anisotropy image (Fig. 3(d)) shows a narrow distribution of anisotropy values around the peak at 0.215 (histogram, Fig. 3(f)). Importantly, there is also no discernible difference in the anisotropy values between the junctions and the perinuclear regions. As a control we measured HBEC expressing empty vector monomeric GFP and found that the average anisotropy value in the cells, r = 0.308 ± 0.012 compared with r = 0.214 ± 0.048 at cell-cell junctions in HBEC expressing CAR-GFP (Fig. 3(i)). These values indicate the presence of a population of fluorophores in the cells expressing CAR-GFP undergoing more rapid depolarization than monomeric GFP, and this is attributed to rapid depolarization via non-radiative energy transfer between GFP units, i.e. homo-FRET.

By using the parallel and perpendicular fluorescence decays from all pixels in the summed series of the measured orthogonally polarized fluorescence images we constructed the time-resolved anisotropy decay (Fig. 3(g)). The decay can be fitted well using a monoexponential

#243733 Received 29 Jun 2015; revised 16 Aug 2015; accepted 18 Aug 2015; published 8 Sep 2015
(C) 2015 OSA

function giving an apparent rotational correlation time of 5.99 ± 1.16 ns, and a limiting anisotropy, r_∞ = 0.15 ± 0.01, indicative of homo-FRET between adjacent GFP units. The existence of homo-dimers or higher order oligomers can decrease the measured anisotropy decay time due to energy transfer between adjacent fluorophores. The r_∞ is then related to the number of GFPs taking part in homo-FRET. Non-radiative resonance energy transfer between adjacent GFP units occurs more rapidly than the rotation of a dimeric/multimeric units leading to more rapid depolarization of the fluorescence than would be seen by rotation alone – an effect which has been exploited for study of protein structure [14] and cluster sizes [13]. It should also be noted that a monoexponential fit to the data is based on the assumption that the rotational correlation time of the constituent GFP units is much longer than the depolarization time due to homo-FRET. Although our time windows for GFP decay measurements are long enough to measure complete GFP fluorescence decays, little Brownian rotational motion takes places during the excited state lifetime. In this case the value of r_∞ is influenced by the proportion of monomeric GFP units in the measured volume. In a system including monomers and oligomers with the oligomers undergoing homo-FRET, the anisotropy increases with an increasing proportion of monomers [69]. The value of r_∞ has also been seen to decrease with increasing cluster size and can be used as a measure of cluster size in some cases [13]. Our data is therefore consistent with the hypothesis that CAR exists predominantly in non-monomeric complexes in living epithelial cells, and that this is not restricted to junctions between adjacent cells.

The representative FRAP recovery curve (Fig. 3(h)) measured from the junction ROI outlined as a red circle in Fig. 3(a) shows an incomplete fluorescence recovery and an immobile fraction of ~85%. This is indicative of CAR that is tethered at the junction either through homo-dimerization in *cis* or *trans*, or potentially through interactions with other scaffold proteins. Interestingly, the immobile fraction of CAR measured here is remarkably similar to that of the classical adherens junction receptor E-cadherin [70] suggesting adhesion receptors can exhibit similar dynamics at cell-cell junctions or that these receptors are functionally linked as we have previously suggested [66]. The representative recovery curve for the CAR-GFP can be adequately fitted using a monoexponential recovery function, with a recovery half-time, $t_{1/2}$ = 145 ± 25 s.

Polarization and time-resolved fluorescence decay data is recorded in every frame of the FRAP recovery, yielding polarization-resolved FRAP recovery curves. The curves measured for the rh123 in solution (Fig. 4(a)) and the tight junction CAR-GFP (Fig. 4(c)) are markedly different due to the faster recovery of the fluorescence in the dye solution and the higher number of photons in the ROI. Using these curves it is possible to measure the anisotropy in the bleached ROI as the fluorescence recovers. As expected, the value of the anisotropy in the ROI for the dye solution is invariant (Fig. 4(b)) due to the uniform distribution of dye molecules and constant viscosity throughout the sample, while the anisotropy can be seen to decrease as a function of recovery time in the CAR-GFP sample (Fig. 4(d)). We measure this decrease by summing the fluorescence intensity in the ROI for ten adjacent frames in both parallel and perpendicular polarization detectors, and we calculate the error in the anisotropy measurements based on the number of detected photons using the treatment presented by Lidke et al. [71] The time-dependent steady-state anisotropy decrease can be fitted well to a monoexponential decay function with a decay time equal to that measured for the FRAP recovery curve.

Variations in steady-state anisotropy as a function of the fraction of the fluorophores in the ROI which has been bleached have been presented by other authors [19, 69]. For the case of randomly distributed monomeric units in the region of interest the anisotropy should remain constant during photobleaching. For a system undergoing FRET photobleaching of acceptor molecules increases the measured anisotropy. CAR-GFP molecules within the ROI are photobleached during the FRAP experiment. During our measured fluorescence recovery unbleached CAR-GFP diffuses into the ROI. We attribute the overall decrease in the anisotropy as a function of time during the recovery to an increase in the proportion of GFP units undergoing FRET, with dimeric/oligomeric units diffusing into the ROI. We note also

#243733 Received 29 Jun 2015; revised 16 Aug 2015; accepted 18 Aug 2015; published 8 Sep 2015
(C) 2015 OSA

that the fluorescence lifetime in the ROI remains invariant during the recovery (Fig. 4(d), inset) which is an indication that there is no fluorescence quenching occurring as the local concentration of unbleached fluorophores increases.

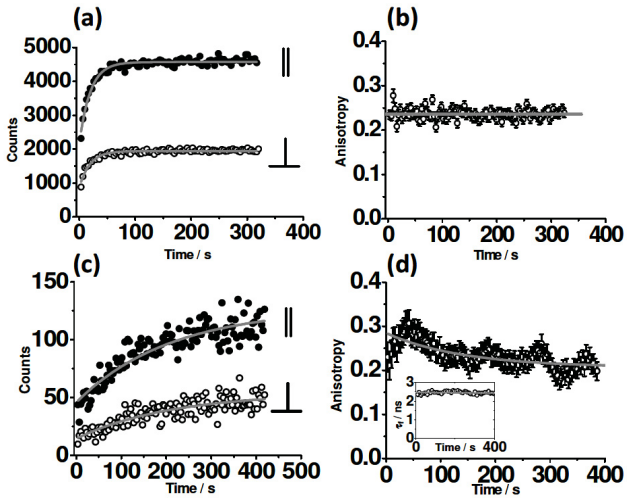

Fig. 4. Measurements of anisotropy in the photobleached ROI during the FRAP recovery. Polarization-resolved FRAP recovery curves for (a) rh123 in a 90% V/V glycerol-methanol mixture and (c) CAR-GFP in living HBEC cells. The black dots represent the recovery of the fluorescence with a polarization parallel to the excitation, and the black circles represent the fluorescence recovery at perpendicular orientation. The recovery curves were used to create plots of anisotropy vs recovery time in the photobleached ROI for (b) rh123 in a 90% V/V glycerol-methanol mixture, which was invariant during the fluorescence recovery and (d) CAR-GFP in living HBEC cells, which decreased during the fluorescence recovery due to transport of GFP units undergoing homo-FRET into the ROI while the fluorescence lifetime stays constant (inset).

4. Discussion

Fluorescence microscopy techniques offer a minimally invasive means of extracting steady-state and dynamic properties of intracellular environments. Individually, FRAP measurements can report on translational protein mobility and binding, and time-resolved fluorescence anisotropy measurements can report on rotational mobility and clustering. The translational diffusion coefficient is influenced by the viscosity of the medium, the size of the mobile unit, and crowding of the environment which reduces the mean free path. The fluorescence anisotropy is also influenced by the viscosity of the medium, the size of the rotating unit, and energy transfer. Our experimental arrangement combines these measurements, and additionally measures the fluorescence lifetime in a single, simultaneous measurement. As such, potential ambiguities in the interpretation of independently measured FRAP and anisotropy data are eliminated, and more detailed clustering and binding information can be obtained.

In the case of CAR-GFP, the FRAP recovery reveals information that may otherwise be open to misinterpretation from anisotropy experiments alone. A translationally immobile fraction at the cell-cell junctions due to *trans* dimerisation would also lead to a reduction in rotational mobility at the junctions in comparison to that in the perinuclear regions where it is highly likely that only *cis* dimerisation would occur. However, this is not evident in the anisotropy image or histograms and the large volume of the dimer unit would yield an anisotropy decay component that is too long to measure using GFP emission even if it were freely rotating. Simply knowing the steady-state anisotropy value in an image cannot reveal more complex dynamics occurring due to hindered rotations and depolarization due to energy transfer. Time-resolved fluorescence anisotropy measurements are essential to disentangle

#243733 Received 29 Jun 2015; revised 16 Aug 2015; accepted 18 Aug 2015; published 8 Sep 2015
(C) 2015 OSA

these phenomena and are therefore an important measurement modality integrated into our microscopy set-up. In the case of homo-dimers the homo-FRET contribution to the anisotropy decay is dominant. Similarly, the presence of dimers cannot be unequivocally determined by FRAP measurements. Translational motion can be slowed by crowded or viscous environments as well as an increase in the size of the mobile unit, and an immobile fraction could also be observed for monomeric structures. Equally, anisotropy measurements alone cannot report on the translational mobility of dimers or oligomerized proteins. This highlights the importance of the FRAP component of the measurements to avoid ambiguities and provide a more complete picture of protein behaviour in living cells. Measurement of the fluorescence lifetime of GFP allows for identification of areas where there are variations in the local environment or self-quenching due to high local concentrations. In the case of our experiments the invariant fluorescence lifetime of GFP during the FRAP recovery is suggestive of there being no concentration-dependent fluorescence quenching.

Our combined FRAP, FLIM, tr-FAIM microscopy data show that CAR exists in a non-monomeric state essentially independent of its location – either in perinuclear vesicles or at cell-cell junctions – with a fraction of the population immobile at the junctions. This implies that dimeric complexes are not formed exclusively at the junctions but rather that CAR exists in a multimeric form everywhere in the cell. This has important implications for understanding how CAR is regulated during epithelial cell junction formation, dissolution and response to adenoviral infection. Interestingly, CAR has also recently been shown to undergo clathrin-mediated endocytosis through binding to AP adaptor proteins [72], and our data would also suggest this may occur through internalisation of a dimeric receptor. Our method, outlined here, is highly suited to the analysis of dimeric/oligomeric complexes and transport properties of other receptors, such as G-protein coupled receptors [73], in living cells, and we believe that it represents a valuable addition to the fluorescence microscopy techniques available to study living cells.

5. Conclusion

We have demonstrated the combination of three powerful fluorescence microscopy techniques - FRAP, FLIM, FAIM - in a single experiment. Simultaneously measuring multiple fluorescence parameters over time - namely position, intensity, lifetime and polarization - yields more insight than sequential measurements using multiple techniques as we examine not only the same cell but the same fluorescence signal, from the same pixels at the same time. The method thus maximises the information available from a limited fluorescence photon budget. It can measure complementary properties required for a comprehensive interpretation of protein dynamics in living cells, which each method on its own cannot provide. We have shown this by measuring the anisotropy as a function of time during a FRAP recovery. This integrated multimodal fluorescence technique thus allows for identification of protein dimers or oligomers and measurement of their translational mobility around the cell. We have demonstrated the power of the technique for monitoring the clustering and dynamics of GFP-tagged cell-cell adhesion molecule CAR, and reveal the fractional preferential multimeric nature of this receptor in intact living cells. Where oligomerization is evident, via low values for fluorescence anisotropy, it is most likely that CAR is interacting in *cis* within intracellular compartments, but both in *cis* and *trans* at cell-cell junctions.

Acknowledgments

We are particularly grateful to Dr. Axel Bergmann of Becker & Hickl GmbH for his valuable assistance with time-resolved image processing, and for providing the OptiSpec software. We also acknowledge Prof. Tony Ng (Randall Division of Cell & Molecular Biophysics and Division of Cancer Studies, King's College London) for valuable discussions. KS would like to acknowledge funding from the UK's Medical Research Council (MRC) and MP funding from the Royal Society and the MRC (MR/K015664/1).

#243733 Received 29 Jun 2015; revised 16 Aug 2015; accepted 18 Aug 2015; published 8 Sep 2015
(C) 2015 OSA